ELSEVIER

Thermochimica Acta 256 (1995) 91–106

thermochimica acta

Nearly stoichiometric iron monoxide formed as a metastable intermediate in a two-stage disproportionation of quenched wüstite. Thermodynamic and kinetic aspects ☆

Svein Stølen *, Ronny Glöckner, Fredrik Grønvold

Department of Chemistry, University of Oslo, Postbox 1033, N-0315 Oslo, Norway

Abstract

Quenched metastable wüstites are shown to undergo a two-stage disproportionation reaction on heating. A mixture of nearly stoichiometric iron monoxide and magnetite is formed during the first stage, which takes place at ≈ 470 K. The resulting nearly stoichiometric $Fe_{1-y}O$ remains metastable up to ≈ 530 K. Above this temperature the stable two-phase mixture of iron and magnetite is slowly formed. The thermodynamic and kinetic aspects of this two-stage disproportionation reaction have been studied in a step-wise heated adiabatic calorimeter. The decomposition behaviour is rationalized in a Gibbs energy of formation representation of stable and metastable phases in the iron–oxygen system. The antiferromagnetic to paramagnetic order–disorder transition which takes place in $Fe_{1-y}O$ at ≈ 196 K is found to be greatly influenced by the oxygen content; it becomes much more cooperative as the exact 1:1 stoichiometry is approached.

Keywords: Disproportionation; Iron monoxide; Kinetics; Stoichiometry; Thermodynamics; Wüstite

☆ Presented at the 14th Symposium on Thermal Analysis and Calorimetry, Oslo, Norway, 15–17 June 1994.

* Corresponding author. Fax: +47 22 85 55 65 or +47 22 85 54 41.

SSDI 0040-6031 (94) 02166-X

1. Introduction

Wüstite is the classical example of a non-stoichiometric phase, and exhibits a maximum iron content equal to approximately $Fe_{0.94}O$ at ≈ 1200 K. The $Fe_{1-y}O$ phase forms eutectoidally from Fe and Fe_3O_4 at ≈ 850 K, is quenchable and remains metastable at room temperature for extended periods of time. The occurrence of a more iron-rich wüstite phase was first reported by Castelliz et al. [1]. According to Fischer et al. [2] the iron-rich wüstite is formed in the first reaction step of a two-stage disproportionation of quenched wüstite. In addition to the new metastable phase the presence of magnetite is also observed. The stable two-phase mixture of iron and magnetite results from the second disproportionation reaction, which takes place at a slightly higher temperature. Although the unit cell dimension of the nearly stoichiometric wüstite phase was found to be independent of the composition of the originally quenched phase [2], it was found to depend on the annealing temperature [3]. The lattice constant decreased from ≈ 432.6 pm for specimens annealed in air below 670 K, to ≈ 430.0 pm for specimens annealed in air at 820 K [3]. The decrease in the lattice constant occurs continuously, and most probably indicates that reoxidiation takes place as the temperature is raised. An "equilibrium" phase diagram as well as a kinetic time–temperature-transformation diagram, indicating the phase limits and the "stability" of the metastable phase, was subsequently proposed [4]. The composition of the nearly stoichiometric wüstite was estimated to be $Fe_{0.99}O$.

In contrast to the seemingly invariant value of the lattice constant observed at ambient temperatures [2–5], various wüstite compositions are formed during the first stage of disproportionation according to Broussard [6]. The lattice constants of the different compositions were, however, determined using only the 220 reflection. For six of the seven specimens with composition between $Fe_{0.995}O$ and $Fe_{0.96}O$ the lattice constant values were 432.1 ± 0.1 pm. It is not clear how the composition of the specimens was determined.

Based on the results of Herai et al. [7], Andersson and Sletnes [8] interpreted the disproportionation results after heat treatment below 570 K in terms of a spinodal decomposition into an iron-deficient and a stoichiometric component. Their conclusion was based on the sequence of morphologies observed after quenching and subsequent short heat treatments by electron diffraction/microscopy. However, the formation of the iron-rich wüstite seems to be intimately connected with the formation of magnetite, as observed by Mössbauer spectroscopy [6] and X-ray diffraction analysis [2,3,9].

The stoichiometry of $Fe_{1-y}O$ is stabilized towards FeO by pressure, and the stoichiometric compound has been synthesized at 1040 K and 36 kbar [10]. The obtained lattice constant [10] is lower than expected from extrapolation of the unit-cell dimension observed for iron-deficient specimens.

The thermodynamics of the wüstite phase in the metastable temperature region can be evaluated from recently reported heat capacities for $Fe_{1-y}O$ from 5 to ≈ 450 K and related results for the stable wüstite phase above the eutectoid temperature [12]. The thermodynamic analysis indicated that on cooling below the

eutectoid temperature the composition of the eutectoid wüstite (as $Fe_{1-x}O_x$) decreases continuously towards stoichiometry ($x = 0.5$). This implies that the stoichiometric compound might form as a reaction intermediate on heating wüstites quenched in ice–brine mixtures. Accordingly, a study of the decomposition mechanism was thought to be of interest.

The reaction mechanism and the thermodynamics of the decomposition of quenched wüstites during heating under vacuum were studied by X-ray diffraction and adiabatic calorimetry. Annealing experiments and subsequent X-ray diffraction analysis were made after establishing the appropriate annealing conditions by adiabatic calorimetry. Adiabatic calorimetry may serve as a very sensitive thermal analysis technique when a step-wise mode of operation is implemented [13]. Different and partly overlapping stages of exothermal reactions can easily pass undetected in the continuous mode of operation, but are readily detected, even in their early stages, when step-wise heating is used. The exothermal enthalpy release gives rise to a positive contribution to the temperature drift rate in the equilibration periods. Hence the detection limit is determined by the temperature drift rate reproducibility of the instrument. Furthermore, controlled preparation of a metastable intermediate is facilitated, as the reaction can be stopped at a suitable stage.

In the present study the composition of the iron-rich phase is estimated on the basis of SQUID measurements and X-ray diffraction results. The effect of the iron content on the magnetic properties of the metastable wüstites is studied by differential scanning calorimetry. Aspects of the magnetic properties are reflected in the heat capacity effects near the order–disorder temperature. The magnetic susceptibility of the wüstites has been reported by Koch and Fine [14], and the heat capacity near the Néel temperature has been determined by adiabatic calorimetry by Todd and Bonnickson for $Fe_{0.947}O$ [15] and by Grønvold et al. for $Fe_{0.9254}O$ and $Fe_{0.9379}O$ [12]. Relative heat capacity measurements on five $Fe_{1-y}O$ samples were reported by Mainard et al. [16].

2. Experimental

2.1. Specimens

The non-stoichiometric wüstites used in this investigation were prepared from iron(III) oxide and iron. The Fe_2O_3 (pro analysi, E. Merck No. 3294) was heated in alumina boats in an electric furnace at 1070 K until constant mass was attained. This required ≈ 40 h and resulted in a mass loss of 0.05%. According to the manufacturer's analysis the impurity limits are (in mass%): Cl^-, 0.01; SO_4^{2-}, 0.01; N, Pb, Cu, Mg, Mn, Ni, Zn, 0.005; insoluble in HCl, 0.01. A spectrographic analysis showed in addition the presence of 50 ppm of SiO_2. A small part of the sample was reduced to pure metallic iron with dry hydrogen gas at 1120 K until the Fe_2O_3/Fe mass ratio was (1.4295 ± 0.0002), theoretical 1.4297. Mixtures of this iron and the Fe_2O_3 with overall Fe/O ratio in the range 0.88–0.95 were heated in

evacuated and sealed vitreous silica tubes at 1270 K for 2 days and furnace cooled. Smaller samples were made for investigation of the decomposition mechanism by annealing and subsequent X-ray diffraction analysis. A larger sample was prepared for the calorimetric investigations.

The oxygen content of the calorimetric sample was determined by oxidation (reduction) of 10–15 g samples at 1070 K in air (H_2) to constant mass in alumina boats. The resulting composition was $Fe_{0.9427}O$. For further details see [12]. The composition of the smaller samples was similarly determined by oxidation and reduction of 0.5 g samples.

The specimens were quenched by dropping them into a water–ice–NaCl solution after heat treatments at 920–970 K for sufficiently long times, usually one to three days.

Room temperature X-ray photographs were taken using the Guinier–Hägg technique with Cr $K\alpha_1$ radiation and Si as an internal calibration substance [17]. High-temperature X-ray diffraction photographs were obtained between 293 and 700 K in an Enraf Nonius (FR 553) Guinier–Simon camera (Cu $K\alpha_1$ radiation, quartz crystal monochromator). The samples were contained in thin-walled sealed silica-glass capillaries. The temperature was controlled via a Pt resistance thermometer and a digital programmer, which synchronized the temperature increase with the movement of the film cassette.

Differential thermal analysis measurements were performed with a Mettler TA 3000 system consisting of a TG10 TA processor and a DSC 30 cell. Magnetic measurements were performed with a SQUID quantum design magnetic measurement system. The specific magnetic moments were calibrated using a standard Pt cylinder as reference sample. The values were adjusted to obtain the correct moment for the NBS standard. The accuracy of the deduced specific magnetic moments is within 1%.

2.2. Calorimetry

The calorimetric apparatus and measuring technique have been described earlier [18,19]. The calorimeter was step-wise heated, and was surrounded by electrically heated and electronically controlled adiabatic shields. A central well in the sample container served for the heater and the platinum resistance thermometer. The thermometer was calibrated locally in the calorimeter at the ice, boiling water, tin, zinc and antimony points. Temperatures are judged to correspond with IPTS-68 to within 0.03 K up to the antimony point and within 0.1 K at 1000 K (the measurements were undertaken before the ITS-90 temperature scale was implemented). The accuracy of the heat capacity measurement is judged to be within 0.5%. The lower accuracy (usually it is within 0.25%) is due to the relatively small samples used in the present investigation. The heat capacity of the ≈ 70 g sample represents $\approx 25\%$ of the total heat capacity of the calorimeter. The heat capacity of the empty calorimeter was determined in a separate series of experiments.

3. Results

3.1. Calorimetry

The heat capacity determinations are presented in chronological order for one mole of quenched (1/1.9427)$Fe_{0.9427}O$ in Table 1 and graphically in Fig. 1. The heat capacities of two-phase mixtures of Fe and Fe_3O_4, and of "FeO" and Fe_3O_4 with overall molar composition (1/1.9427)$Fe_{0.9427}O$, are represented in the same figure by solid and dashed curves, respectively, and the heat capacity of $Fe_{0.9425}O$ is represented by the dotted curve [12]. The latter curve was calculated as the mean of earlier determinations on $Fe_{0.9379}O$ [12] and $Fe_{0.947}O$ [20]. Two separate series of measurements were undertaken. In both cases the measurements on the quenched wüstite could be continued up to ≈ 450 K before the beginning of disproportionation caused an increasing positive temperature drift rate of the calorimeter from one energy input to the next. The individual temperature drift rates in the equilibration period after each energy input are shown in Fig. 2. After some additional energy inputs, the calorimeter was left in order to regain equilibrium. Thermal equilibrium was reached at ≈ 520 K, where the temperature drift rate became equal to the drift rate before the disproportionation reaction was initiated.

At this stage, no significant increase in the calorimeter drift rate was caused by some smaller energy inputs, see Fig. 2. The heat capacity obtained in this temperature region is close to that expected for a two-phase mixture of stoichiometric wüstite and magnetite as shown in Fig. 1. A new reaction, which correponds to a second stage of the disproportionation, started at ≈ 550 K. The calorimeter temperature increased to ≈ 610 K before the reaction approached completion

Table 1
Heat capacity of the quenched (1/1.9427) $Fe_{0.9427}O$ sample

T in K	$C_{p,m}$ in J K^{-1} mol^{-1}	T in K	$C_{p,m}$ in J K^{-1} mol^{-1}	T in K	$C_{p,m}$ in J K^{-1} mol^{-1}
Series I		exotherm	disprop. I	452.70	26.44
315.68	25.36	531.64	27.06	465.19	25.86
326.94	25.53	544.61	27.25	477.16	24.39
338.28	25.57	557.81	27.55	494.52	8.74
350.06	25.68	571.26	27.64	exotherm	disprop. I
362.18	25.95	exotherm	disprop. II	523.74	27.06
374.39	26.03	Series II		529.84	27.11
386.65	25.90	327.58	25.36	535.74	27.05
398.92	26.03	339.10	25.59	541.81	27.08
411.24	25.79	350.64	25.71	548.36	27.47
423.62	25.58	390.19	25.99	563.11	27.91
436.10	25.31	402.73	26.20	exotherm	disprop. II
448.89	24.97	415.35	25.99	623.13	30.73
461.58	24.92	427.77	26.31	636.61	30.95
474.13	23.23	440.21	26.19	650.66	30.46
486.99	13.86				

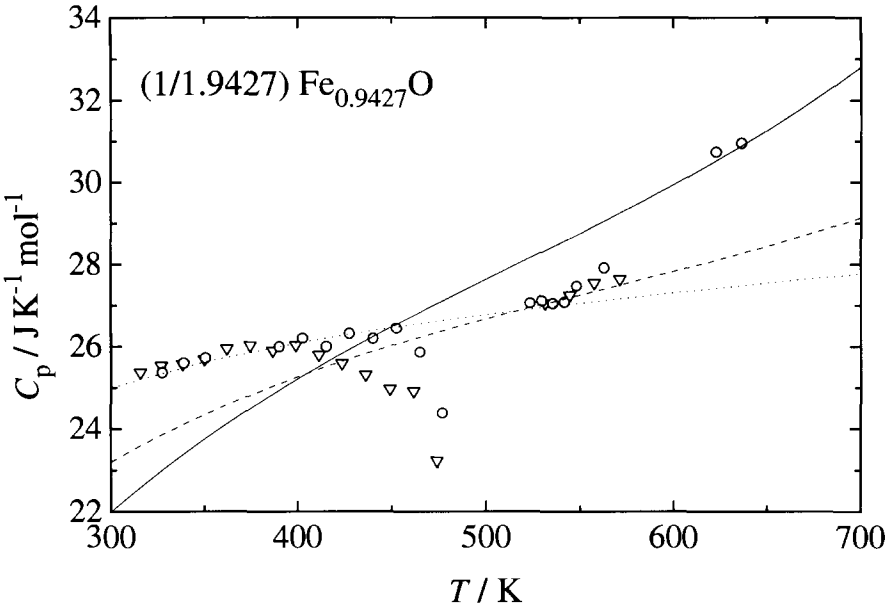

Fig. 1. Molar heat capacity of quenched (1/1.9427)$Fe_{0.9247}O$. △, Series I; ○, Series II; (.....), mean of the heat capacity of (1/1.9379)$Fe_{0.9379}O$ [12] and (1/1.947)$Fe_{0.947}O$ [20]; (-----), and solid line, mixtures with overall composition (1/1.9427)$Fe_{0.9427}O$ consisting of FeO and Fe_3O_4 and of Fe and Fe_3O_4, respectively.

(series II); see Fig. 3. The formation of the stable two-phase mixture proceeded very slowly. Thus, a temperature drift rate of ≈ 3 mK min^{-1} was observed even at ≈ 620 K. Additional energy inputs resulted in an increased temperature drift rate, and hence showed that the reaction was not complete at this stage. X-ray diffraction photographs of samples with identical thermal history confirmed this interpretation; see below. Above 620 K the heat capacity corresponds to that expected for a two-phase mixture of iron and magnetite (see Fig. 1).

The calorimetric experiments thus indicate a two-stage disproportionation. The exothermal enthalpy release connected with the first stage of the disproportionation was measured in two series of experiments, giving $\Delta_{trs}H_m(Fe_{0.9427}O) = -3.3$ and -2.4 kJ mol^{-1}, respectively. For the second disproportionation reaction, ≈ -7.1 kJ mol^{-1} was released during equilibration for 4155 min (series II only).

3.2. X-ray diffraction analysis

Annealing experiments were designed on the basis of the calorimetric experiments, and the results of the investigation are presented in Table 2. Wüstites with composition $Fe_{0.8956}O$, $Fe_{0.9194}O$ and $Fe_{0.9357}O$ were studied. The presently observed lattice constants for the quenched non-stoichiometric wüstites are plotted in Fig. 4, which also contains earlier reported values. An approximately linear relationship between the lattice constant and the mole fraction of oxygen is observed. This

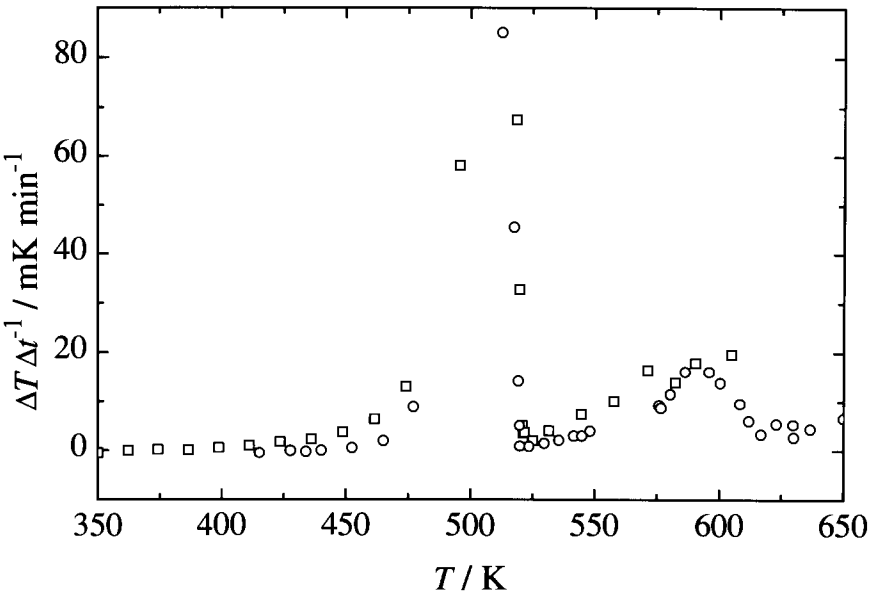

Fig. 2. Individual temperature drift rates after each energy input.

relationship can be used for estimating the composition of quenched wüstites, and also for detecting changes in phase composition after annealing.

For all three compositions, annealing at ≈ 490 K for 6 h resulted in a three-phase mixture of two wüstite phases and magnetite. One of the wüstite phases has a unit cell parameter equal to that observed for the quenched specimens before the heat treatment; the other corresponds to a more iron-rich wüstite. The lattice constant of the latter phase is equal for all three specimens, i.e. the composition of this new phase does not depend on the overall composition of the quenched specimens.

Further annealing at higher temperatures or for longer periods of time, see Table 2, gives rise to a two-phase mixture of the iron-rich wüstite and magnetite, followed by the formation of metallic iron (in a three-phase mixture with the iron-rich $Fe_{1-y}O$ and magnetite). This observation indicates the start of formation of the stable two-phase mixture of iron and magnetite. The second stage of the disproportionation, however, is found to proceed rather slowly, in agreement with the slow approach to equilibrium observed by calorimetry.

A two-stage disproportionation of the quenched specimens is thus observed. The quenched wüstites decompose to the stable two-phase mixture of iron and magnetite through an intermediate stage which gives a metastable two-phase mixture of nearly stoichiometric $Fe_{1-y}O$ and magnetite. The disproportionation reactions have also been followed by high-temperature X-ray diffraction, the two-step nature being confirmed.

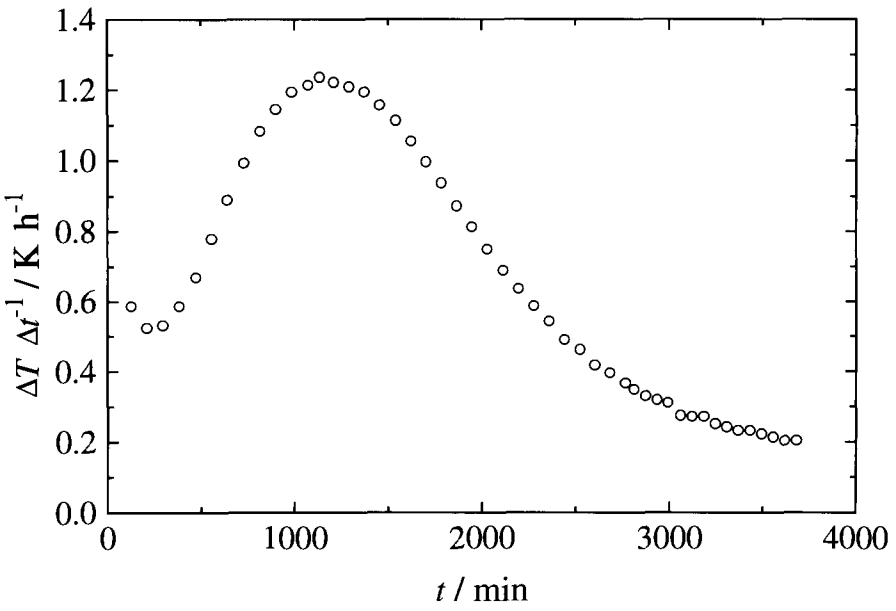

Fig. 3. Temperature drift rate as a function of time showing the spontaneous temperature increments due to the second disproportionation reaction.

3.3. Composition of the intermediately formed metastable phase

The composition of the iron-rich wüstite formed in the first disproportionation reaction when $Fe_{0.9357}O$ is annealed for 24 h at 520 K was derived from determinations of specific magnetic moment. Pure Fe_3O_4 and quenched $Fe_{0.9357}O$ served as reference samples and the three samples were measured at 4 K in magnetic fields up to 4 MA m^{-1}; see Fig. 5(a) and (b). The composition of the iron-rich wüstite can be calculated from the following reaction

$$Fe_{1-y}O = [(4y-1)/(4z-1)]Fe_{1-z}O + [(z-y)/(4z-1)]Fe_3O_4$$

The specific magnetic moment in zero magnetic field was extrapolated from the results in high magnetic fields, and the values for Fe_3O_4, $Fe_{0.9357}O$ and the two-phase mixture were 96.5, 0.0 and 18.3 A m^2 g^{-1}, respectively. The composition derived for the nearly stoichiometric phase (calculated assuming two phases present only) is then $Fe_{0.99}O$. This value corresponds with that derived from the observed lattice constant value $a = 432.5$ pm; see Fig. 4.

The present observations will be investigated further by precision calorimetry at low temperatures, including the region of the magnetic order–disorder transition in the magnetite, in order to provide more quantitative information.

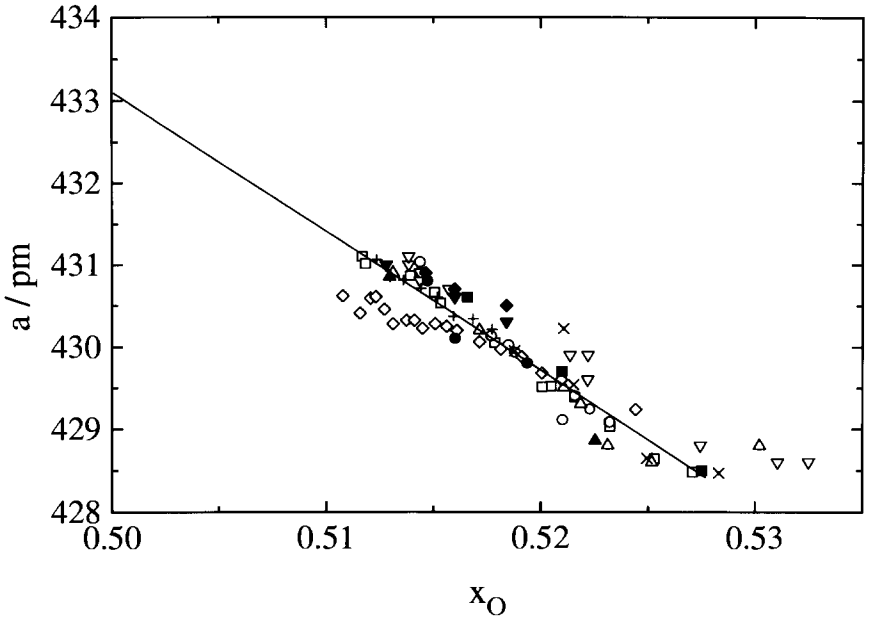

Fig. 4. Lattice constants of quenched wüstites at ambient temperature. ○, Jette and Foote [11]; □, Levin and Wagner [21]; △, Touzelin [9]; ▽, Marion [22]; ◇, Carel [23] quenched from 1613 K; +, Carel [23] quenched from 1473 K; ×, Bredesen and Kofstad [24]; ●, Grønvold et al. [12]; ▲, Foster and Welch [25]; ▼, Seehra and Srinivasan [26]; ◆, Battle and Cheetham [27]; ■, present results.

3.4. Magnetic characterization using differential scanning calorimetry

The degree of cooperation of the magnetic order–disorder transition of $Fe_{1-y}O$ is reflected in the shape of the heat capacity curve in the temperature region around 196 K, where the antiferromagnetic to paramagnetic transition occurs. In the present study, quenched wüstite samples with composition $Fe_{0.8797}O$, $Fe_{0.8956}O$, $Fe_{0.9194}O$, $Fe_{0.9255}O$, $Fe_{0.9357}O$ and $Fe_{0.9427}O$ have been studied by the DSC technique. The results for two selected, representative specimens are presented in Fig. 6 together with heat flow results for the calorimetric sample recorded after it had been through the first stage of the disproportionation reaction. Clearly, the transition becomes much more cooperative when the exact 1:1 stoichiometry is approached.

4. Discussion

4.1. Disproportionation mechanism

The X-ray diffraction results presented in Table 2 for the isothermally heat treated wüstite samples indicate that the heat treatment results in the simultaneous

Table 2
X-ray analysis of specimens quenched and subsequently annealed. The lattice constant (in pm) of the cubic wüstite phase is given

T in K	t in h	$Fe_{1-y}O$ non-stoichio.	$Fe_{1-y}O$ near stoichio.	Fe_3O_4	Fe
$Fe_{0.8956}O$					
as quenched		428.5	no	no	no
370	6	428.5	no	no	no
470	6	428.1	no	no	no
490	6	429.0 [a]	432.1	yes	no
500	6	no	432.1	yes	no
520	24	no	432.4	yes	no
520	72	no	432.2	yes	yes
$Fe_{0.9194}O$					
as quenched		429.7	no	no	no
370	6	429.5	no	no	no
470	6	429.4	no	no	no
500	6	429.7	432.5	yes	no
520	24	no	432.8	yes	no
520	72	no	432.5	yes	yes
$Fe_{0.9357}O$					
as quenched		430.6	no	no	no
370	6	430.6	no	no	no
420	6	430.6	no	no	no
470	6	430.6	432.7	yes	no
520	24	no	432.5	yes	no
520	72	no	432.4	yes	yes

[a]Large uncertainty due to line broadening.

formation of stoichiometric wüstite and magnetite. For short heat treatments at lower temperatures (e.g. 6 h at 470–500 K) two distinct wüstite phases are observed. One of the wüstite phases has a lattice constant which is equal to that for the quenched specimen before the heat treatment; the other is larger and corresponds to a more iron-rich composition. With increasing duration of the heat treatment, the intensity ratios of corresponding X-ray reflections from the two phases increase in favour of those from the larger unit cell.

These observations are at variance with the spinodal type decomposition mechanism proposed by Andersson and Sletnes [8]. This was based on the morphology of the specimens after much shorter heat treatments than in the present study (typically 20 min at 570 K). Magnetite was not observed in their experiments, except on surface layers and in some of the most iron-deficient specimens. The actual composition of the two wüstite phases was not determined. It is not clear whether Andersson and Sletnes [8] observed regions with different sub-lattice constants, i.e. different compositions, or if their observations regarding

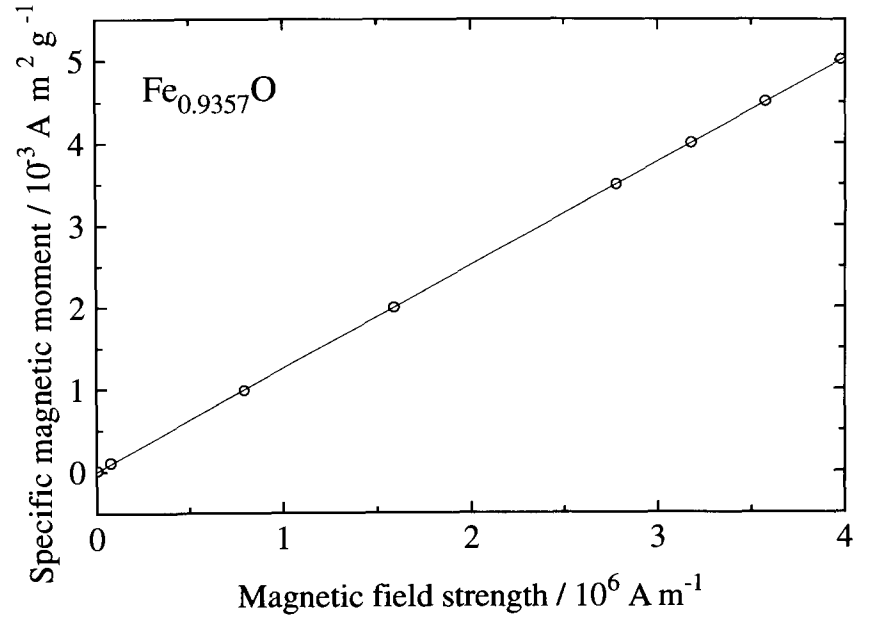

(a)

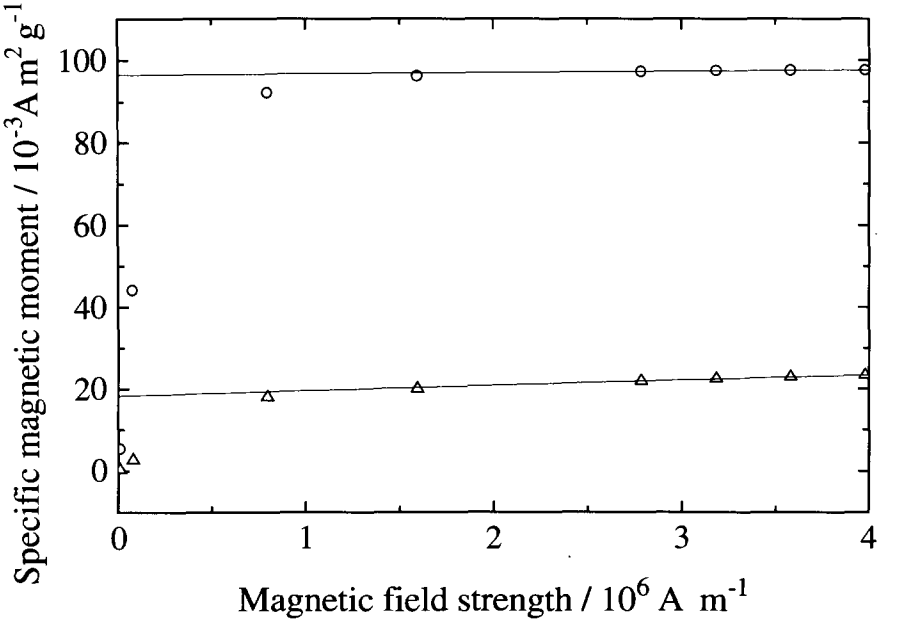

(b)

Fig. 5. Specific magnetic moment as a function of magnetic field strength: (a) results for quenched $Fe_{0.9357}O$; (b) results for the intermediately formed two phase mixture (△) and for magnetite (○).

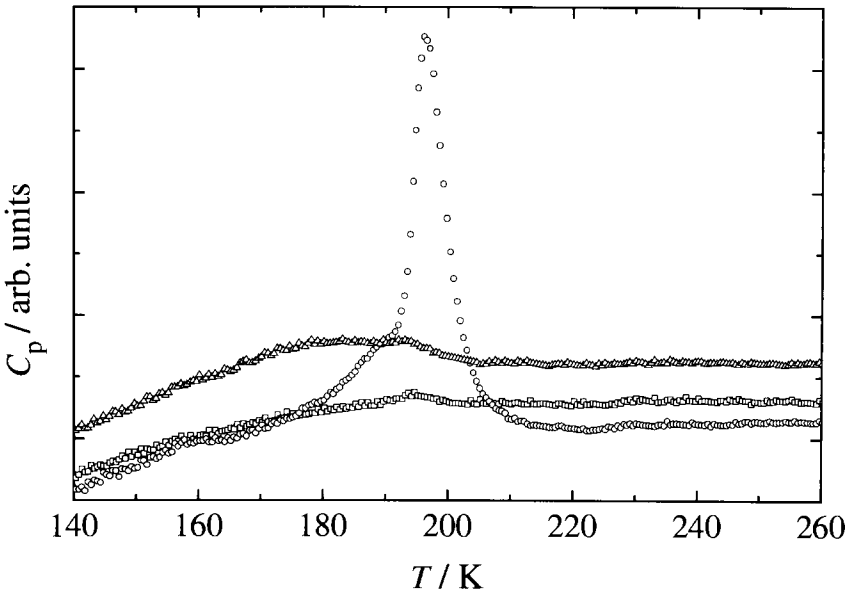

Fig. 6. Heat flow rate near the magnetic order–disorder transition for $Fe_{0.9427}O$ (△), $Fe_{0.9255}O$ (□) and the intermediately formed two-phase mixture of nearly stoichiometric wüstite and magnetite (○). The zero point for each curve is arbitrarily chosen.

the presence of stoichiometric wüstite were related to the absence of superstructure formation.

The present investigation indicates a reaction mechanism different from the spinodal one [8]. It stems from the observation that the composition of the originally quenched specimen does not change during the first stage of the disproportionation around 470 K. It might be argued that the iron-deficient wüstite obtained is unstable and rapidly undergoes further disproportionation to the iron-rich wüstite and magnetite. From this point of view the invariant lattice constant merely indicates that the phase is not fully disproportioned. The morphologies reported in the electron microscopy study [8] appear to form readily, and the spinodal type decomposition should thus be detectable by adiabatic calorimetry. Nevertheless, no exothermal enthalpy effect was observed below ≈ 470 K in the present study.

The mechanisms of the disproportionation reaction can be discussed in terms of schematic Gibbs energy of formation diagrams. The compositional dependence of the Gibbs energy of formation for the wüstite phase is exaggerated compared with the actual situation; see [12], for example. A diagram corresponding to a spinodal type decomposition is presented in Fig. 7. The representation suggests a three-stage disproportionation. In the first stage disproportionation within the wüstite phase results in the formation of two wüstite phases with different compositions. The iron-deficient wüstite decomposes into the iron-rich modification and magnetite in

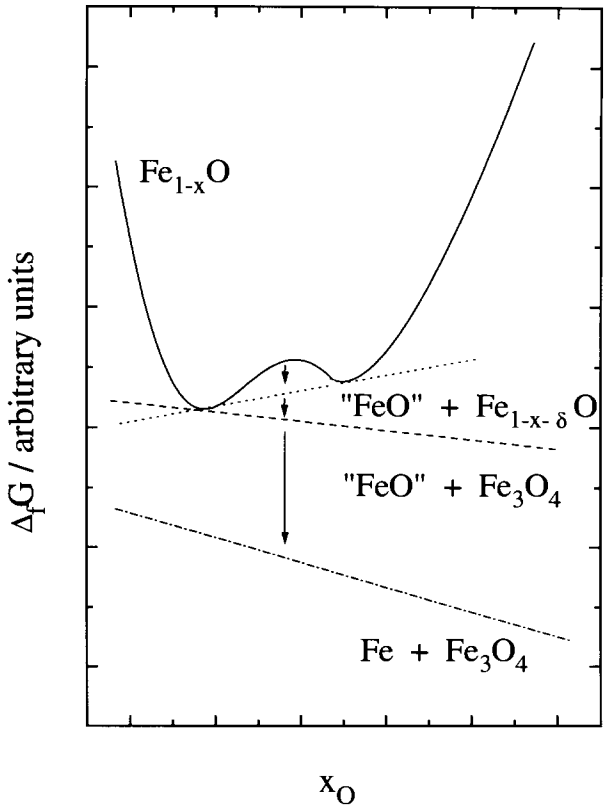

Fig. 7. Schematic diagram of the Gibbs energy of formation for the relevant phases in the Fe–O system at e.g. 500 K. Spinodal type decomposition.

the second stage, whereas the stable two-phase mixture of iron and magnetite is formed in the final reaction. An alternative disproportionation mechanism which leads to the formation of an intermediate metastable two-phase mixture is shown in Fig. 8. Here the formation of a metastable two-phase intermediate product results in the occurrence of an iron-rich wüstite simultaneously with the exsolution of magnetite. The present results favour the latter model, which presumably represents the approach to the "equilibrium" situation, where the reactions taking place in the specimens are governed by the successive decrease in Gibbs energies of formation of the different metastable modifications. The creation of various ordered superstructures depending upon the heating rate in a non-equilibrium situation is not surprising. For such cases the reaction steps may show a much more complex pattern as a result of variations in thermal history.

Early stage spinodal decomposition can, however, not be completely ruled out, as magnetite was not observed by Andersson and Sletnes.

The decomposition mechanism can be understood on the basis of two main effects. A recent thermodynamic analysis indicates that on cooling below the

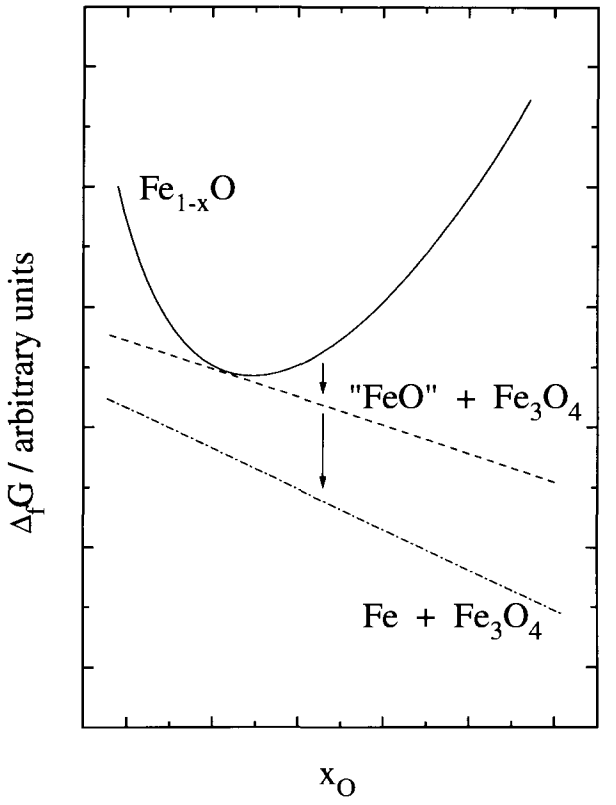

Fig. 8. Schematic diagram of the Gibbs energy of formation for the relevant phases in the Fe–O system at e.g. 500 K. Decomposition with formation of a metastable intermediate.

eutectoidal temperature the composition of metastable eutectoid wüstite (as $Fe_{1-x}O_x$, with $x > 0.5$) changes continuously towards stoichiometry ($y = 0.5$). This observation relates to the occurrence of wüstites with larger lattice constants in some earlier studies, and thus to compositions closer to stoichiometry, and suggests that the stoichiometric composition might result if the annealing were to take place at a suitably low temperature. In the present study, no variation in the lattice constant of the iron-rich wüstite was observed as result of changes in annealing conditions from 430 K for three weeks to 520 K for 24 h. Earlier annealing experiments [4] in air at > 620 K resulted in decreasing lattice constants, which were probably caused by oxidation.

A second possible cause for the increased stability of the iron-rich wüstite is the diminishing effect of the disorder entropy on the Gibbs energy as the temperature is lowered. Hence minima in the Gibbs energy are expected in regions where favourable defect structures of the wüstite phase may occur as a result of stronger bonding. This implies that a minimum in Gibbs energy which corresponds almost to a stoichiometric compound may develop at low temperatures.

Based on the mechanism proposed above, as well as on the recent thermodynamic analysis of wüstite [12], the exothermal reaction enthalpy for the second stage of the disproportionation is expected to be ≈ -9.4 kJ mol^{-1} if the intermediately formed phase is assumed to be stoichiometric. This indicates that $\approx 75\%$ of stoichiometric FeO has disproportionated after 4155 min at ≈ 620 K in our experiment (only -7.1 J mol^{-1} was released). As the iron content of the iron-rich phase most probably is slight below stoichiometric, a somewhat larger fraction of the specimens is completely decomposed to iron and magnetite. The exothermic enthalpy value connected with this second stage of the disproportionation is, however, uncertain, because of the finite instrumental temperature drift rates which become important at long equilibration periods.

4.2. The magnetic order–disorder transition

The heat capacity near the Néel temperature for specimens with different compositions has been studied by adiabatic calorimetry by Todd and Bonnickson [15] and by Grønvold et al. [12]. The studies differ in one important respect. The heat capacity effect observed by Todd and Bonnickson for a sample with composition $Fe_{0.947}O$ [15] is much larger than those observed for the slightly more iron-deficient specimens $Fe_{0.9254}O$ and $Fe_{0.9379}O$ [12]. In the present study, results are presented both for single-phase specimens with composition from $Fe_{0.90}O$ to $Fe_{0.9427}O$ and for specimens consisting of Fe_3O_4 and the intermittently formed iron-rich wüstite. Only very small heat effects are observed in the Néel temperature region for the original as-quenched samples. In contrast, a large heat capacity effect is observed for the two-phase $Fe_3O_4 + Fe_{0.99}O$ sample. Thus, the transition in wüstite becomes much more cooperative when the composition approaches stoichiometry. The large heat capacity effect observed by Todd and Bonnickson [15] probably indicates that a small amount of nearly stoichiometric wüstite was present in their sample, which was the same as previously used by Coughlin et al. in their drop calorimetric study [20]. Unfortunately, the thermal history of the sample was not given.

Acknowledgement

The authors thank the Norges Forskningsråd for financial support.

References

[1] L. Castelliz, W. de Sutter and F. Halla, Monatsh. Chem., 85 (1954) 487.
[2] W.A. Fischer, A. Hoffmann and R. Shimada, Arch. Eisenhüttenwes., 27 (1956) 521.
[3] W.A. Fischer and A. Hoffmann, Arch. Eisenhüttenwes., 30 (1959) 15.
[4] A. Hoffmann, Z. Elektrochem., 63 (1959) 207.
[5] W.A. Fischer and A. Hoffmann, Arch. Eisenhüttenwes., 29 (1958) 107.
[6] L. Broussard, J. Phys. Chem., 6 (1969) 1848.

[7] T. Herai, B. Thomas, J. Manenc and J. Benard, C. R. Acad. Sci., 258 (1964) 4528.
[8] B. Andersson and J.O. Sletnes, Acta Crystallogr., Sect. A, A33 (1977) 268.
[9] B. Touzelin, Rev. Int. Hautes Temp. Refract., 11 (1974) 219.
[10] T. Katsua, B. Iwasaki, S. Kimura and S. Akimoto, J. Chem. Phys., 47 (1967) 4559.
[11] E.R. Jette and F. Foote, J. Chem. Phys., 1 (1933) 29.
[12] F. Grønvold, S. Stølen, P. Tolmach and E.F. Westrum, Jr., J. Chem. Thermodyn., 25 (1993) 1089.
[13] S. Stølen and F. Grønvold, High Temp.-High Press., 25 (1993) 161.
[14] F.B. Koch and M.E. Fine, J. Appl. Phys., 38 (1967) 1470.
[15] S.S. Todd and K.R. Bonnickson, J. Am. Chem. Soc., 73 (1951) 3894.
[16] R. Mainard, M. Boubel and H. Fousse, C.R. Acad. Sci., Ser. B, 266B (1968) 1299.
[17] R.D. Deslattes and A. Henins, Phys. Rev. Lett., 31 (1973) 972.
[18] F. Grønvold, Acta Chem. Scand., 21 (1967) 1695.
[19] F. Grønvold, J. Chem. Thermodyn., 25 (1993) 1133.
[20] J.P. Coughlin, E.G. King and K.R. Bonnickson, J. Am. Chem. Soc., 73 (1951) 3891.
[21] R.L. Levin and J.B. Wagner, Jr., Trans. AIME, 236 (1966) 516.
[22] M.F. Marion, Doc. Metall., 24 (1955) 87.
[23] C. Carel and J.R. Gavarri, Mater. Res. Bull. 11 (1976) 745.
[24] R. Bredesen and P. Kofstad, Oxid. Met., 36 (1991) 27.
[25] P.K. Foster and A.J.E. Welch, Trans. Faraday Soc., 52 (1956) 1626.
[26] M.S. Seehra and G. Srinivasan, J. Phys. C: Solid State Phys., 17 (1984) 883.
[27] P.D. Battle and A.K. Cheetham, J. Phys. C: Solid State Phys., 12 (1979) 337.